



Age softening phenomenon and microscopic mechanism of Li–B alloy

Hai-feng HUANG, Zhi-Jian LIU, Chao-ping LIANG, Li-bao CHEN

State Key Laboratory of Powder Metallurgy, Central South University, Changsha 410083, China

Received 14 March 2020; accepted 4 June 2020

Abstract: The age softening phenomenon of the Li–B alloy was investigated by a series of tensile tests under various aging conditions. The results show that the tensile strength of the rolled Li–B alloy decreases with increasing aging time. Higher aging temperature accelerates the softening process, and leads to an early end of aging. A model was proposed to analyze the mechanism of the age softening. The vacancy annihilation is the control factor of age softening. The strength–temperature relationship was estimated by the newly proposed model and a standard heat treatment, annealing at 150 °C for 1 h, was designed to eliminate the age softening of rolled Li–B alloy.

Key words: thermal battery; Li–B alloy; age softening; lithium metal battery; lithium dendrite

1 Introduction

Thermal battery is a type of primary batteries, which uses molten salts as electrolytes and employs an internal pyrotechnic (heat) source to bring the battery stack to operating temperatures [1]. Because thermal batteries have virtually no self-discharge, they can be stored for more than 25 years [2] and brought into operational service immediately. This is useful in applications that need a long shelf life with no maintenance, high power density, or a ruggedization, such as guided weapon systems, proximity fuzes in ordnance devices, and space flights [2]. In order to make sure the fact that the loaded weapon can endure the severe mechanical movement (higher acceleration, shock, spin, vibration, etc.), the disks, including electrode disk, electrolyte disk and pyrogenetic disk, must be tightly assembled [3]. Therefore, each type of the material in the battery must be consistent in mechanical properties, especially after long time (over 25 years) storage, which is another requirement besides the electrochemistry requirement.

Lithium–boron (Li–B) alloy is a new generation anode material for thermal battery [4]. It is a two-phase composite which consists of a pure Li matrix and a lithium boride (LiB) skeleton [5], similar with “LAN” technology that is pure lithium in a metallic matrix. WANG [4,6] proposed the preparation method of Li–B alloy. In the past decades, a new Li–B alloy has been successfully developed and its electrochemical performance [7–9] in the molten salts system and mechanical properties [10] were systematically studied. However, the reliability of the thermal battery using Li–B alloy anode after a long shelf time for 25 years, has not been carefully investigated.

The mechanical reliability of the Li–B alloy is one of the crucial factors to ensure safe operation of the thermal batteries. Especially, after long shelf time, the accumulated change in physical properties would cause catastrophic result. The melting point of Li is only 180.5 °C and its recrystallization temperature is as low as 20 °C [11]. The mechanical strength can be evolved obviously during the storage stage under ambient conditions (typically, from –55 to 75 °C) [2]. The small size and relative light atom mass of Li element facilitate

the self-diffusion of Li–B alloy and thus may promote the evolution of mechanical properties. If the morphological porous structure and chemical composition of Li–B skeleton are affected, the adsorption ability of the Li–B skeleton to liquid Li matrix will be influenced, which may cause the breakdown of thermal battery due to the outflow of liquid Li. In recent years, the Li–B alloy has shown great potential as anode material for lithium–sulfur batteries [12–14], lithium metal batteries [15,16] and lithium solid state batteries [17]. The mechanism of the dendrite generation and the mechanical behavior are related to the movement of the Li atoms and the distribution state of different defects. So, the study on the mechanical mechanism of the Li–B alloy would bring out valuable information that will be helpful for the understanding of the Li dendrite generation mechanism [16].

In this work, in order to ensure the stability and reliability of Li–B alloy materials used in batteries, we revealed the tensile strength of Li–B alloy at different temperatures and aging time, and analyzed the intrinsic mechanism. An analytical model based on the vacancy annihilation and Li self-diffusion was proposed and applied to predicting the age softening of Li–B alloy. A heat treatment process, annealing at 150 °C, was later designed to accelerate the age softening to stable state. Besides, the phase composition, thermal stability and discharge stability of Li–B alloy were investigated as a supplement for validation of the reliability of Li–B alloy. Through the above work, we discovered and revealed the mechanism of age softening of Li–B alloys, and provided standard heat treatment methods to solve softening problems. By means of the model presented in this work, the reason why the Li–B anode could display better ability to resist dendrite formation in lithium metal battery system was also well explained.

2 Experimental

Commercialized Li–B alloy was supplied by State Key Laboratory of Powder Metallurgy (Central South University, Changsha, Hunan, China), with a lithium nominal content of 61 wt.% with a certain amount of magnesium (Mg) addition.

The tensile test was carried out on the Li–B alloy under four conditions: (1) the sample was

sealed in vacuum glass tube and aged at 100, 20 and 0 °C (marked as Conditions A, B and C, respectively); (2) the sample was first sealed with paraffin in tin can under argon atmosphere, wrapped in aluminum-plastic foil sealed bag, and aged at 20 °C (marked Condition D). It should be noted that Condition D is the commercial pack way of the Li–B alloy. The four samples were aged for different periods of time and followed by tensile test.

The tensile sample was 0.4 mm in thickness, with a standard distance of $L_0=30$ mm. The tensile test was conducted at room temperature with a strain rate of 10 mm/min.

The phase composition of Li–B alloy was studied by X-ray diffractometry (XRD) using a Rigaku D/max 2550PC with Cu K_α radiation ($\lambda=1.54056$ Å). A scanning speed of 8 (°)/min and an interval of 0.02° were adopted during the test.

The morphology of the LiB skeleton was observed by scanning electron microscope (SEM) using JSM–6360LV instrument. For one week immersing of the Li–B alloy in a solution of 8 wt.% naphthalene in tetrahydrofuran [18], the free lithium can be removed from the alloy and then the LiB skeleton sample was prepared.

The electrochemical performance of Li–B alloy was performed according to the method by XIE et al [19] and NING et al [20]. Li–B alloy disk of 0.4 mm in thickness and 17.5 mm in diameter was used as the anode. The electrolyte is 50 wt.% LiF–LiCl–LiBr (9.6 wt.%, 22 wt.%, 68.4 wt.%) salt and 50 wt.% MgO binder [19]. The cathode contained 80 wt.% CoS_2 and 20 wt.% the electrolyte. The electrolyte and the cathode powder were put in the upper and lower layers together in a die, and were pressed at a pressure of 250 MPa. The diameter of the composite disk of electrolyte and cathode was also 17.5 mm. The anode and the composite disk of electrolyte/cathode were assembled into a single cell. The final cell was subjected to galvanostatic discharge (500 mA/cm²) at the operation temperature of 520 °C.

3 Results and discussion

3.1 Phase composition and morphology

The phase compositions of as-cast and rolled Li–B alloy were characterized by XRD. Figure 1 shows a typical two-phase XRD pattern which

consists of metal Li phase and LiB compound phase. As shown in Fig. 1(a), the as-cast Li-B alloy is the sample block directly taken out of the cast ingot. The XRD pattern of the rolled sample (Fig. 1(b)) has evident difference with that of the as-cast sample. The LiB (101) diffraction peak at 2θ value of 41° disappears, and the intensities of LiB (100) and (110) peaks increase largely. This is due to the alignment of the LiB along the rolling direction, implying a strong texture structure formed in LiB skeleton [5]. In general, deformation has a significant effect on the mechanical properties of materials [21]. It must be pointed out that the Li-B alloy strip of 0.4 mm in thickness was cold-rolled from the thick plate blank with the thickness over 40 mm, which means a high working rate of 10000% attained and the enormous working defects accumulated in Li-B alloy strip.

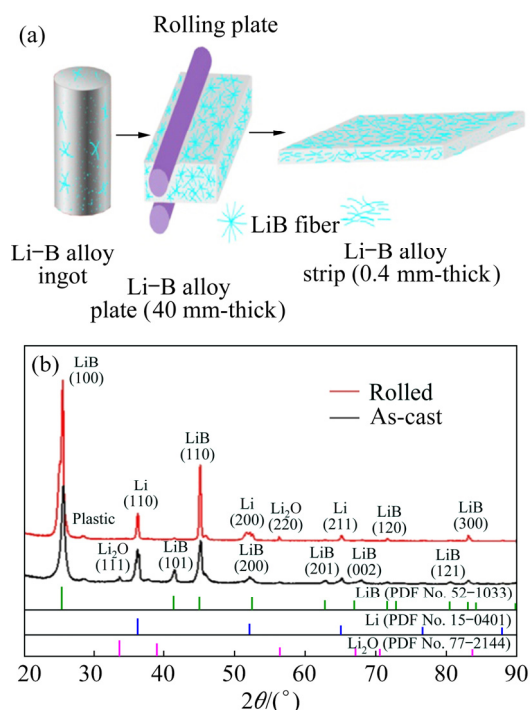


Fig. 1 Schematic plot of processing of Li-B alloy (a) and XRD patterns of as-cast and rolled Li-B alloys

Figure 2 shows the morphologies of LiB fibers by removing Li matrix. The morphology of the LiB skeleton confirms the texture explanation deduced from XRD patterns. The orientation distribution of LiB skeleton fibers is different from that of the as-cast and rolled samples of which is arranged almost in parallel. It is found that the diameter of the LiB skeleton is about 0.5 μm . Hereinafter, only the rolled Li-B alloy was used for tensile test, and

the Li-B alloy was referred to the rolled Li-B alloy without specification.

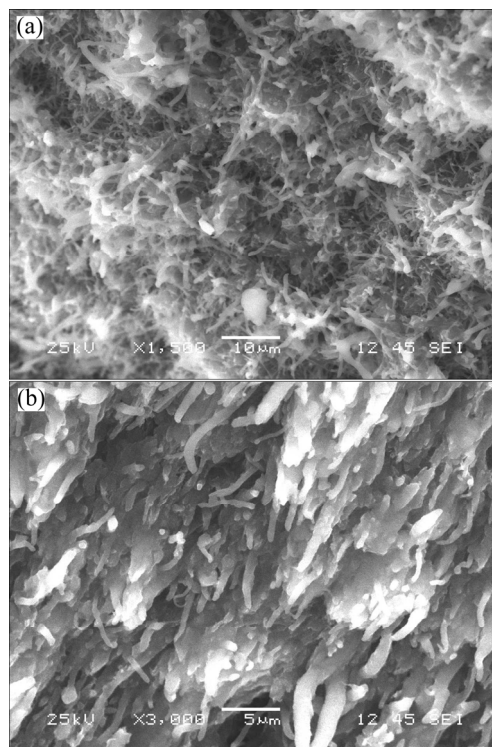


Fig. 2 Morphologies of LiB fibers by removing Li matrix: (a) As-cast Li-B alloy; (b) Rolled Li-B alloy

3.2 Age softening phenomenon

Figure 3 shows a typical stress-strain curve of Li-B alloy. The rolled Li-B alloy, a composite material composed of Li matrix and LiB fibers, has no obvious yield point and shows good plasticity.

The tensile strength of Li-B alloy undergoing various aging time and temperature is shown in Table 1 and Fig. 4. The strength of all samples decreases to a constant value as function of aging time. For example, the strength of Sample B first

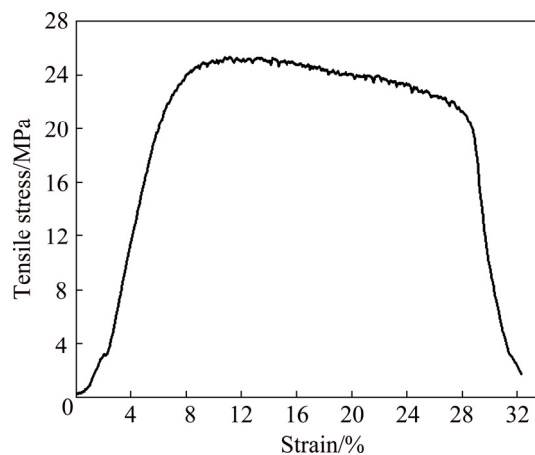
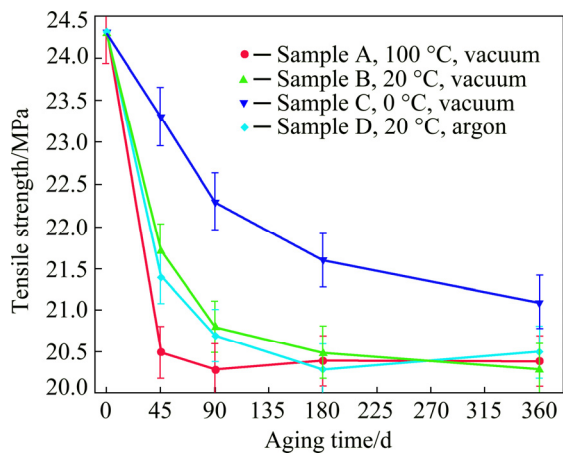


Fig. 3 Typical tensile stress-strain curve of Li-B alloy

Table 1 Tensile strength of Li–B alloy under different conditions

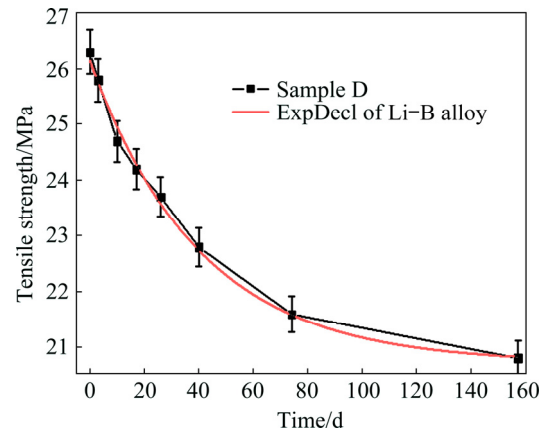
Aging time/d	Tensile strength/MPa				
	Initial	Sample A	Sample B	Sample C	Sample D
0	24.3	–	–	–	–
45	–	20.5	21.7	23.3	21.4
90	–	20.3	20.8	22.3	20.7
180	–	20.4	20.5	21.6	20.3
360	–	20.4	20.3	21.1	20.5

**Fig. 4** Tensile strength of Li–B alloy as function of aging time

drops to 21.7 MPa after aging for 45 d, and reaches to a constant value around 20.5 MPa at aging time over 180 d. This is similar to the typical recovery phenomenon for metals/alloys with cold working [22]. According to the recovery theory, the aging temperature determines the recovery speed and extent. The higher the aging temperature is, the faster the strength decreases. However, there is a lower boundary for the strength value at aging temperature higher than 20 °C. The strength of Samples A and B, being aged at 100 and 20 °C, respectively, has almost the same strength after 360 d, even though the strength of Sample A goes down sharply at the beginning of recovery.

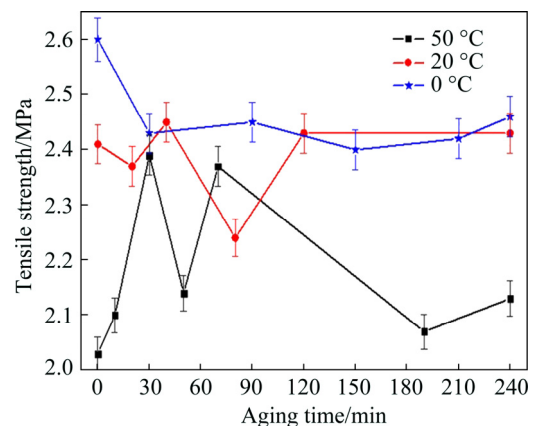
A dense sampling of tensile test was conducted to gain a deep insight of the strength decay of Li–B alloy. Figure 5 shows the strength of Sample D at 20 °C with respect to aging time. The tensile strength shows an exponential decay as a function of aging time. The relationship between tensile strength and aging time was fitted by Eq. (1):

$$\sigma = 20.7 + 5.4 \exp(-t/40.5) \quad (1)$$

**Fig. 5** Exponential function fitting of tensile strength of Sample D with respect to aging time

where σ is the tensile strength (MPa), and t is the aging time (d). A correlation coefficient $R^2=0.99$ is satisfied after fitting, indicating a perfect exponential decay behavior.

To investigate the role of the LiB skeleton fiber in the tensile strength decay, an aging experiment was performed on the Li matrix as well. The tensile strength of the rolled Li matrix is shown in Fig. 6. Counter intuitively, the rolled Li matrix which is strengthened by Mg addition shows almost no age softening. The LiB skeleton fibers have played a key role in the age softening of Li–B alloy.

**Fig. 6** Tensile strength of Li matrix as function of aging time at different temperatures

If there is a direct observation on the microstructure of the age softening process, then the discussion on the mechanical mechanism investigation of the composite material will be deeper and more direct. We have made great efforts to finish the transmission electron microscope (TEM) test. However, the alloy sample

is not able to bear the high-speed electron bombardment, so the TEM experiment had to be cancelled.

3.3 Modeling of age softening mechanism

The experimental results show that there is no the age softening phenomenon for the pure solid solution of lithium and magnesium, which indicates that the dislocation and vacancy generated by rolling at room temperature with large deformation have recovered at the same time. So, the age softening phenomenon caused by the recovery correlation will not be shown. After deep rolling, the LiB fibers in the alloy are arranged in parallel along the rolling direction. The fiber is bound in covalent bond with the melting point up to 1000 °C [5], so its property should be stable. The uniform high-density distribution of LiB skeleton fiber in the alloy will greatly hinder the recovery of dislocation and vacancy. Therefore, the tensile strength is greatly improved at room temperature with the tensile strength of 2.3 MPa for Li–Mg solid solution rising to 27 MPa for Li–B alloy, which is still 20 MPa after age softening. In this case, it can be thought that the reinforcement yielded by LiB fiber distribution does not cause age softening, but reinforcement caused by delayed vacancy defects due to the LiB fiber can be attenuated by aging. As pointed out before, the Li matrix has a recrystallization temperature lower than room temperature [11]. The mechanical behavior of the Li–B alloy at room temperature should be equivalent to that of general high temperature alloy, so the mechanical mechanism could be similar to that of the high temperature alloy. In other words, vacancy defects should play a key role in the strength mechanism of Li–B alloys.

For the Li–B alloy, the LiB skeleton fibers, most of them aligned after rolling direction, could pin the dislocations and then promote work hardening in the Li–B alloy, as shown in Fig. 7(a). Calculation shows that the Li–B alloy has 30 vol.% LiB fibers and the average diameter of LiB fibers is about 0.5 μm . Then, the calculated average distance between LiB fibers is about 1.2 μm . This distance is shorter than normal dislocation length in Li matrix, indicating a strong pinning effect of dislocation (Fig. 7(a)). In addition, the low melting point of Li matrix would entail excess Li vacancies in the Li matrix.

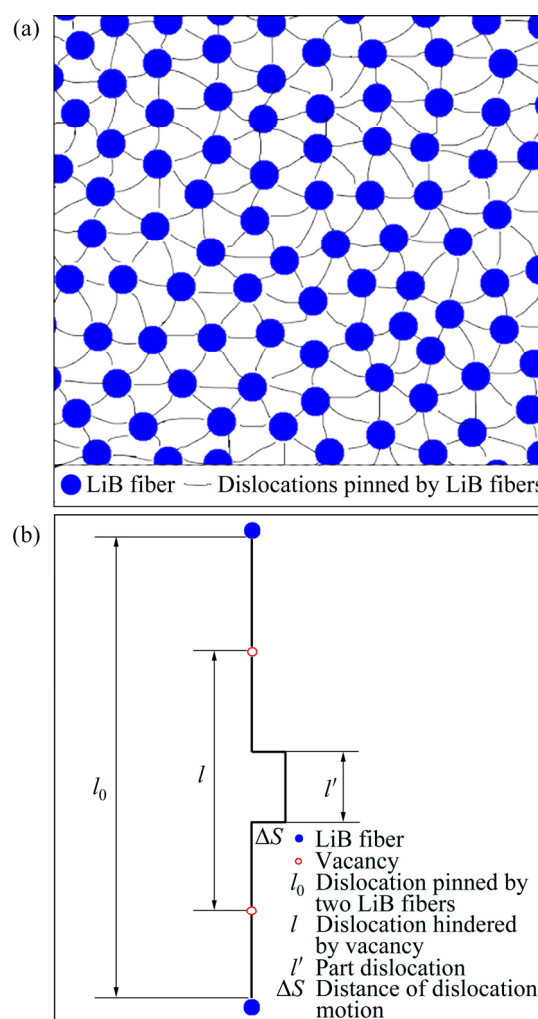


Fig. 7 Schematic diagrams of interaction between generated dislocations and LiB fibers in Li–B alloy (a), and dislocation motion with assistance of vacancy annihilation (b)

Based on the results of existing experiments, we proposed a model to explain the age softening of Li–B alloy. The main idea is as follows: the LiB fibers pin the dislocation generated during rolling; the excess vacancy migration and annihilation take place during the aging time; the vacancies resist the migration and recombination of dislocation. Owing to the thermal activation action, the vacancy densities decrease with increasing aging time and speed up with increasing aging temperature, which eventually results in the decrease or softening of the strength of Li–B alloy.

An analytical model was derived according to the above idea. As shown in Fig. 7(b), we consider a linear dislocation l_0 which is pinned by two LiB fibers at the end points. Part of the dislocation l is

further pinned by two vacancies. Inside l , a kink l' pops up on the slip plane from thermal activation. At last, the corresponding macro-strain of the sample (ε) is proportional to the area swept by dislocation l motion:

$$\varepsilon = klb \quad (2)$$

where b is the Burgers vector component, and k is a constant related to the slip plane and the direction of the kink. The strain rate is calculated by

$$\dot{\varepsilon} = klv \quad (3)$$

with

$$v = v_0 \exp[-\Delta G_1 / (RT)] \quad (4)$$

where v is the effective jump frequency of dislocation l' , v_0 is the equilibrium background jump frequency, ΔG_1 is the activation energy required to activate dislocation movement, R is the mole gas constant, and T is the thermodynamic temperature.

As shown in Fig. 8(a), when there is no stress applied, the left and right jump rates of the dislocations are equal, and there is no net strain rate,

$$\dot{\varepsilon} = klv_0 \{ \exp[-\Delta G_1 / (RT)] - \exp[-\Delta G_1 / (RT)] \} = 0 \quad (5)$$

Under stress, as shown in Fig. 8(b), the left and right jump rates of dislocations are biased, and the strain rate is

$$\dot{\varepsilon} = klv_0 \{ \exp[-(\Delta G_1 - \Delta G'_1) / (RT)] - \exp[-(\Delta G_1 + \Delta G'_1) / (RT)] \} \quad (6)$$

with

$$\Delta G'_1 = \sigma l' b \Delta s / 2 \quad (7)$$

where $\Delta G'_1$ is the additional energy required for dislocation motion under stress, and Δs is the distance of dislocation line motion. Equation (6) can be rewritten as

$$\dot{\varepsilon} = klv_0 \exp[-\Delta G_1 / (RT)] \{ \exp[\Delta G'_1 / (RT)] - \exp[-\Delta G'_1 / (RT)] \} \quad (8)$$

Using Taylor expansion, we take the first two terms and get

$$\dot{\varepsilon} = klv_0 \exp[-\Delta G_1 / (RT)] \cdot \{ [1 + \Delta G'_1 / (RT)] - [1 - \Delta G'_1 / (RT)] \} \quad (9)$$

Considering there are N atomic positions around the dislocations and there are n vacancies, the l_0 can be divided into $n+1$ segments by those n vacancies. The relationship between l and l_0 is

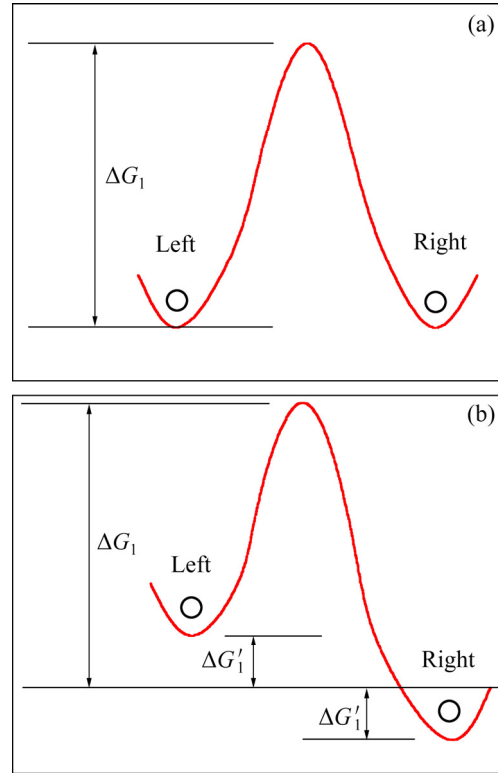


Fig. 8 Activation energy of dislocation motion without stress (a) and with stress (b)

$$l = l_0 / (n+1) \quad (10)$$

According to the statistical distribution, we have the following relationship based on the vacancy concentration C , atomic positions N' and vacancies n' in the matrix, and atomic positions N and vacancies n around the dislocations,

$$C = n' / N' = n / N \quad (11)$$

Putting Eq. (11) into Eq. (10), we get

$$l = l_0 / (CN+1) \quad (12)$$

Therefore, the strain rate of Eq. (9) can be rewritten as

$$\dot{\varepsilon} = 2k \frac{l_0}{CN+1} v_0 \exp[-\Delta G_1 / (RT)] \frac{\sigma l' b \Delta s}{RT} \quad (13)$$

with constant strain rate condition in the tensile test, $\dot{\varepsilon}$ is equal to constant $\dot{\varepsilon}$, then

$$C = 2 \frac{kl_0}{\dot{\varepsilon}_0 N} v_0 \exp[-\Delta G_1 / (RT)] \frac{\sigma l' b \Delta s}{2RT} - \frac{1}{N} \quad (14)$$

For a given system, according to Eq. (14) the vacancy concentration can determine the stress σ . As time increases, the vacancy concentration decreases, so the stress σ decreases. The stress σ on

the slip plane is proportional to the tensile strength σ_b :

$$\sigma_b = g\sigma = g \frac{\dot{\epsilon}_0 (NC + 1)}{kl_0 b v_0 \exp[-\Delta G_1 / (RT)] l' b \Delta s} \frac{RT}{\quad} \quad (15)$$

where g is a factor related to the critical resolved shear stress.

It can be seen from Eq. (15) that the tensile strength of the alloy is inversely proportional to the average spacing of the LiB skeleton fibers, which is also the average length of the pinned dislocation line and proportional to the vacancy concentration C . With the prolonging of aging time, the age softening phenomenon occurs owing to the decrease of the vacancy concentration during recovery. Finally, the vacancy concentration tends to be constant, and the remained reinforcement by the LiB skeleton fibers will not further decrease with the extension of aging time.

The vacancy concentration decrease rate is proportional to the vacancy concentration

$$dC/dt = k'C \quad (16)$$

where k' is a constant determined by the diffusivity of vacancy. The vacancy annihilation rate v' is controlled by the self-diffusion of vacancy:

$$v' = v'_0 \exp[-\Delta G_2 / (RT)] \quad (17)$$

where ΔG_2 is the self-diffusion activation energy of vacancy annihilation. k' can be replaced by v' ,

$$dC/dt = v'_0 \exp[-\Delta G_2 / (RT)] C \quad (18)$$

Taking the logarithm of both sides of Eq. (18), we get

$$d \ln C / dt = v'_0 \exp[-\Delta G_2 / (RT)] \quad (19)$$

By putting Eqs. (14) and (15) into (19), we have

$$d \ln \sigma_b / dt = v'_0 \exp[-\Delta G_2 / (RT)] \quad (20)$$

where σ_b is the ultimate stress. Integrating both sides of Eq. (20), the ultimate stress is

$$\ln \sigma_b = v'_0 \exp[-\Delta G_2 / (RT)] t + B \quad (21)$$

$$\sigma_b = \sigma_{b0} \exp\{v'_0 \exp[-\Delta G_2 / (RT)] t\} \quad (22)$$

At different temperatures, if the strength decays to a given value, Eq. (22) can turn into Eq. (23) by taking logarithm twice:

$$\ln t = A + \frac{\Delta G_2}{RT} \quad (23)$$

where A is a constant. It can be deduced from

Eq. (23) that the self-diffusion activation energy of vacancy annihilation, ΔG_2 , can be obtained from the slope of a line of time and temperature.

As we have ascribed the strength decay to the vacancy annihilation, we would expect a very low ΔG_2 . The ΔG_2 was calculated by fitting the experimental data into Eq. (23). Figure 9 shows the linear fitting results of Li–B alloy. The ΔG_2 is only 23 kJ/mol for Li–B alloy, which is much smaller than 53 kJ/mol of Li self-diffusion in pure lithium metal in Ref. [23]. The small ΔG_2 supports our assumption that vacancy annihilation is the main reason of the age softening.

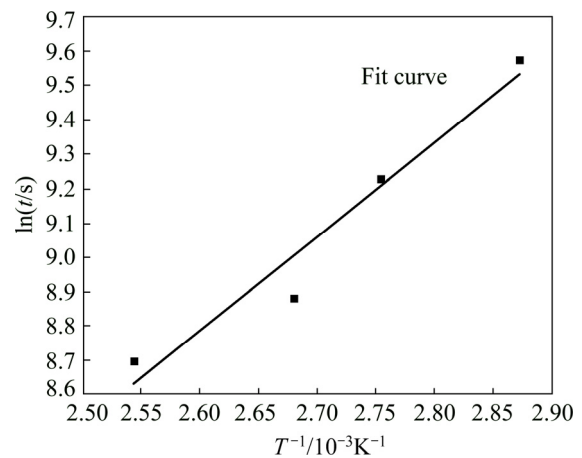


Fig. 9 Linear fitting of $\ln t$ and T^{-1} based on age softening data of Li–B alloy

The reason for lower activation energy in Li–B alloy is two aspects. Firstly, the vacancy annihilation is an energetically favorable process. After rolling, the Li–B alloy is at a high energy state with many pinned dislocations and vacancies. The dislocations provide short-circuit pathways for Li self-diffusion, thus leading to much lower diffusion activation energy [22]. Secondly, the addition of Mg facilitates the vacancy migration by enlarging the lattice. Mg has a larger atomic size than Li. Adding Mg in to Li matrix will increase the lattice spacing for Li diffusion. In this case, lower activation energy of the Li atom diffusion is attained.

3.4 Acceleration treatment of age softening

The above model can help us understand the age softening of Li–B alloy, and can be used to design a heat treatment to accelerate the age softening of the Li–B alloy. As stated in the introduction, the mechanical stability influences the

long shelf time and operation reliability of thermal battery. In order to quickly eliminate age softening and meet application requirements, the higher the temperature is, the faster the Li–B alloy reaches a stable state. The heat treatment temperature should not exceed the melting point of lithium, so 150 °C is a more suitable temperature. Based on Eq. (23) and the calculated activation energy ΔG_2 , we derived that annealing at 150 °C for 1 h can accelerate the age softening of Li–B alloy to the end. To validate our theoretical prediction, we designed a comparison experiment of which two rolled Li–B alloys are divided into two groups: one is aged at room temperature for 30 d, the other is annealed at 150 °C for 1 h.

The tensile strength of these two samples is listed in Table 2. The experimental results confirm our theoretical prediction. The tensile strength of the sample annealed at 150 °C for 1 h is almost the same as that of the sample aged at room temperature for 30 d followed by annealing. It should be noted that the tensile strength of the sample aged at room temperature for 30 d decreases from 25.2 to 23.6 MPa. This is consistent with our assumption that there is strength change after long time room temperature storage and then potential quality defect of the thermal battery appears after long-term storage. As a result, we proposed to standardize this annealing process for the Li–B alloy used for thermal battery.

Table 2 Tensile strength of aged and annealed Li–B alloys (MPa)

Initial	Aged at RT for 30 d	Annealed at 150 °C for 1 h
25.2	23.6	21.7
25.1	–	21.5

Since 150 °C is close to the melting point (180.5 °C) of Li, the side reaction at 150 °C should be evaluated before the standardization of this heat treatment process. Consequently, the XRD was performed for the pristine, annealed and aged samples, and the results are shown in Fig. 10. It can be seen that the XRD patterns of the pristine sample, the sample aged at room temperature for 30 d and the sample annealed at 150 °C for 1 h have no discernible difference, which indicates that the phase composition of Li–B alloy has not been

changed during heat treatment, in particular, annealing. Therefore, it can be confirmed that the state of the Li–B alloy is not changed before and after various heat treatments.

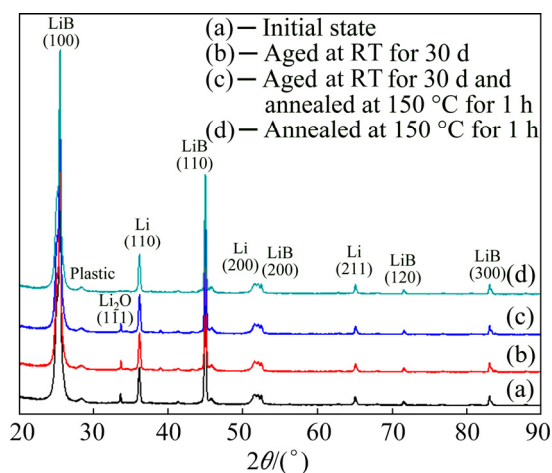


Fig. 10 XRD patterns of pristine, aged and annealed Li–B alloy

3.5 Thermal stability evaluation

Thermal stability, the ability of LiB skeleton absorbing liquid Li matrix at high temperature, is the most important indicator of the Li–B alloy. To the best of our knowledge, there is no existing method for characterizing thermal stability in the industry. An effective thermal stability test was presented here. A Li–B alloy disk (17.5 mm in diameter and 0.4 mm in thickness), packed in aluminum silicate ceramic fiber paper, was enclosed in a heating block and hold at 600 °C for 5 min. If the fiber paper is etched and the alloy ignites, it indicates that the LiB skeleton has poor adsorption performance for liquid Li matrix, as the liquid Li matrix flows out and reacts with air exothermally. If the surface of the fiber paper is intact, it indicates that LiB skeleton absorbs and fixes liquid Li matrix well.

Figure 11 shows the photos of the Li–B alloy after thermal stability test. The thermal stability test results of Li–B alloy at annealed state and aged at room temperature for up to 1000 d show that the surface of ceramic fiber paper is intact as that tested at that day, implying that Li–B alloy could withstand the high temperature test at 600 °C. The above tests revealed that the Li–B alloys either annealed or aged for a long time keep good thermal stability. Therefore, these results strongly support

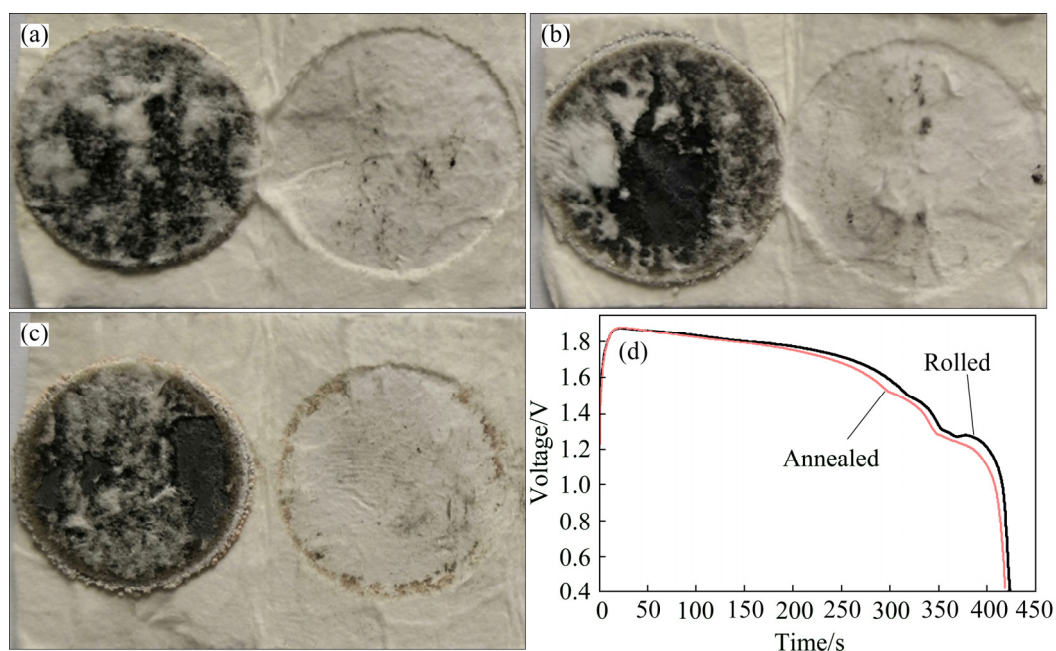


Fig. 11 Photos of thermal stability test of Li–B alloy at aging time of 0 d (a) and 1000 d (b), after being annealed (c) and discharge curve of rolled and annealed Li–B alloys at galvanometric current density of 500 mA/cm² (d)

that the strength change of Li–B alloy does not affect its thermal stability under high temperature required by thermal battery. This also means that the adsorption characteristics of liquid Li matrix into LiB skeleton are not changed, and the microstructure of LiB skeleton is not altered. Furthermore, it can be inferred that age softening does not affect the high-temperature discharge performance of the Li–B alloy.

The initial and annealed Li–B alloys were subjected to discharge at 500 mA/cm², and the results are shown in Fig. 11(d). It can be seen from Fig. 11(d) that the shape of the discharge curve is basically the same, the voltage is close, and the discharge time is equivalent. This shows that there is no obvious difference in electrochemical properties of the two-state Li–B alloys.

3.6 Mechanism for lithium dendrite of Li–B alloy and pure Li metal anode for Li–S and Li metal batteries

In recent years, there have been many researches on using Li–B alloy as the substitute of the lithium anode for lithium–sulfur battery [12–14], and most of the papers showed positive results. The porous LiB skeleton played an import role in increasing the effective anode area during charging and discharging and then reduced the deposition

speed of the Li atoms, thus effectively inhibiting the formation of lithium dendrite on the anode.

Recently, we have found that the addition of Mg to Li–B alloys inhibits the generation of Li dendrites more effectively [16]. The above analysis showed that the diffusion coefficient of the Li atoms in the Li–B alloy will be about 1.6×10^5 times higher than that in the pure Li anode. With the concepts derived above, we can investigate the effect of high diffusion rate on suppressing the formation of lithium dendrites. Dendrite nucleation is the result of the competition between the inhomogeneous deposition of lithium and the flattening caused by interfacial tension of metal/electrolyte.

At first, the small inhomogeneous protrusion takes place on the Li deposition surface due to thermal fluctuation and other factors. Then, on the protrusion surface there is a compressive stress which will extrude the Li atoms out of this area to the flatten area. But the atoms have to overcome the activation energy barrier before growing to the outside. In other words, it depends on the diffusion rate of the Li atoms in the alloy. When the diffusion rate is greater than the deposition rate of lithium, the dendrite nucleation of lithium cannot be completed, and vice versa.

According to the above results, the diffusion

rate of lithium atoms in Li–B alloy is increased by nearly 100000 times, so the formation of lithium dendrites is significantly inhibited in this case. The promotion of the diffusion rate of lithium atoms greatly improves the dynamic conditions of the formation of lithium dendrites, as shown in Fig. 12, showing that the alloying of lithium metal is an important way to reduce the formation of lithium dendrites.

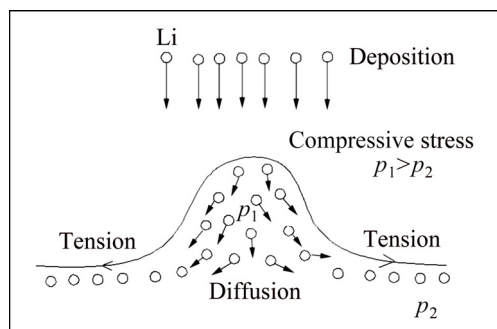


Fig. 12 Li diffusion and Li dendrite suppression of Li–B alloy

4 Conclusions

(1) The as-rolled Li–B alloy strip has an exponential decay on the tensile strength with the increase of aging time and temperature (age softening).

(2) An analytical model was presented for the age softening of Li–B alloy. The vacancy annihilation and related Li self-diffusion are responsible for the age softening, which is accompanied by the decrease of vacancy defect.

(3) By means of the model, Li self-diffusion activation energy of Li–B alloy is calculated to be 23 kJ/mol.

(4) Based on the model, a standard heat treatment, annealing at 150 °C for 1 h, was proposed to accelerate age softening to end.

(5) Experiments show that age softening and annealing do not influence the phase composition, thermal stability and discharge stability of Li–B alloy.

(6) The lower Li self-diffusion activation energy of Li–B alloy has an effect on preventing the dendrite from formation in lithium metal battery.

Acknowledgments

The authors thank Prof. Min SONG for the useful discussion on the mechanical mechanisms.

References

- [1] NIU Yong-qiang, ZHU Wu, DU Jun-lin, PU Chao-hui. Discharge behavior of Li–Mg–B alloy/MnO₂ couples with LiNO₃–KNO₃–Mg(OH)NO₃ eutectic electrolyte [J]. *Electrochimica Acta*, 2014, 115(3): 607–611.
- [2] GUIDOTTI R A, MASSET P J. Thermally activated (thermal) battery technology. Part I: An overview [J]. *Journal of Power Sources*, 2006, 161(2): 1443–1449.
- [3] MASSET P J, GUIDOTTI R A. Thermal activated (thermal) battery technology. Part II: Molten salt electrolytes [J]. *Journal of Power Sources*, 2007, 164(1): 397–414.
- [4] WANG F E. An unusual phenomenon in the formation of Li₅B₄ compound-alloy [J]. *Metallurgical Transactions A*, 1979, 10(3): 343–348.
- [5] LIU Zhi-jian, QU Xuan-hui, HUANG Bai-yun, LI Zhi-you. Crystal structure and morphology of a new compound, LiB [J]. *Journal of Alloys and Compounds*, 2000, 311(2): 256–264.
- [6] WANG F E. Metal alloy and method of preparation thereof: US patent, 4110111 [P]. 1978–8–29.
- [7] LIU Zhi-jian, QU Xuan-hui, LI Zhi-you, HUANG Bai-yun. Mechanism of reaction synthesis of Li–B alloys [J]. *Science in China Series E: Technological Sciences*, 2003, 46(4): 391–400.
- [8] LIU Zhi-jian, LI Zhi-you, DUANG Wei, QU Xuan-hui, HUANG Bai-yun, ZHANG Si-qi. Preparation of Li–B alloy and study of its microstructure and discharge characteristics [J]. *Journal of Materials Science & Technology*, 2000, 16(6): 581–584.
- [9] LIU Chao, LIU Zhi-jian, HUANG Hai-feng, WEN You-cai. Discharge characteristics of lithium-boron anode in molten salt battery [J]. *Chinese Journal of Power Sources*, 2014, 38(4): 717–720. (in Chinese)
- [10] HUANG Hai-feng, LIU Zhi-jian, YANG Xiao-liang, WANG Hui, WEN You-cai. Mechanical property of Li–B alloy used for anode materials of thermal battery [J]. *Chinese Journal of Materials Research*, 2010, 24(2): 187–190. (in Chinese)
- [11] ZHANG Mi-lin, YAN Yong-de. *Lithium and lithium alloys* [M]. Beijing: Science Press, 2015. (in Chinese)
- [12] DUAN Bo-chao, WANG Wei-kun, ZHAO Hai-lei, WANG An-bang, WANG Meng-jia, YUAN Ke-guo, YU Zhong-bao, YANG Yu-sheng. Li–B alloy as anode material for lithium/sulfur battery [J]. *ECS Electrochemistry Letters*, 2013, 2(6): A47–A51.
- [13] CHENG Xin-bing, PENG Hong-jie, HUANG Jia-qi, WEI Fei, ZHANG Qiang. Dendrite-free nanostructured anode: Entrapment of lithium in a 3D fibrous matrix for ultra-stable lithium–sulfur batteries [J]. *Small*, 2014, 10(21): 4257–4263.
- [14] ZHANG Xiao-lin, WANG Wei-kun, WANG An-bang, HUANG Ya-qin, YUAN Ke-guo, YU Zhong-bao, QIU Jing-yi, YANG Yu-sheng. Improved cycle stability and high security of Li–B alloy anode for lithium–sulfur battery [J]. *Journal of Materials Chemistry A*, 2014, 2(30): 11660–11665.
- [15] LIU Qiang, ZHOU Si-si, TANG Cong, ZHAI Qiao-ling, WANG Rui. Li–B alloy as an anode material for stable and

- long life lithium metal batteries [J]. *Energies*, 2018, 11(10): 2512.
- [16] WU Chen, HUANG Hai-feng, LU Wei-yi, WEI Zeng-xi, NI Xu-yan, SUN Fu, QING Piao, LIU Zhi-jian, MA Jian-min, WEI Wei-feng. Mg doped Li–LiB alloy with in situ formed lithiophilic LiB skeleton for lithium metal batteries [J]. *Advanced Science*, 2020, 7(6): 1902643.
- [17] ZHONG Hai, SANG Lin, DING Fei, SONG Jiang-xuan, MAI Yao-hua. Conformation of lithium–aluminium alloy interphase-layer on lithium metal anode used for solid state batteries [J]. *Electrochimica Acta*, 2018, 277: 268–275.
- [18] KILROY W P, ANGRES I. The extraction and determination of free lithium in Li–B alloys [J]. *Journal of the Less-Common Metals*, 1979, 63(1): 123–128.
- [19] XIE You-long, LIU Zhi-jian, NING Hui-long, HUANG Hai-feng, CHEN Li-bao. Suppressing self-discharge of Li–B/CoS₂ thermal batteries by using a carbon-coated CoS₂ cathode [J]. *RSC Advances*, 2018, 8(13): 7173–7178.
- [20] NING Hui-long, LIU Zhi-jian, XIE You-long, HUANG Hai-feng. CoS₂ coatings for improving thermal stability and electrochemical performance of FeS₂ cathodes for thermal batteries [J]. *Journal of the Electrochemical Society*, 2018, 165(9): A1725–A1733.
- [21] MA Yun-long, LI Jin-feng, ZHANG Run-zhe, TANG Jian-guo, HUANG Cheng, LI Hong-ying, ZHENG Zi-qiao. Strength and structure variation of 2195 Al–Li alloy caused by different deformation processes of hot extrusion and cold-rolling [J]. *Transactions of Nonferrous Metals Society of China*, 2020, 30(4): 835–849.
- [22] LAUGHILIN D E, HONO K. *Physical metallurgy* [M]. 5th ed. Amsterdam: Elsevier, 2014.
- [23] LODDING A, MUNDY J N, OTT A. Isotope inter-diffusion and self-diffusion in solid lithium metal [J]. *Physica Status Solidi*, 2010, 38(2): 559–569.

锂硼合金的时效软化现象及其微观机制

黄海锋, 刘志坚, 梁超平, 陈立宝

中南大学 粉末冶金国家重点实验室, 长沙 410083

摘要: 通过不同时效条件下的拉伸试验, 研究锂硼合金的时效软化现象。结果表明, 随着时效时间的延长, 轧制锂硼合金的抗拉强度明显下降; 高温可加速此软化过程, 使锂硼合金提前进入稳定状态。在此基础上, 提出时效软化模型, 揭示空位湮灭是时效软化的控制因素。利用该模型得到合金强度–温度的关系, 并制定一个标准热处理方法, 即在 150 °C 退火 1 h, 可快速消除锂硼合金的时效软化现象。

关键词: 热电池; 锂硼合金; 时效软化; 锂金属电池; 锂枝晶

(Edited by Wei-ping CHEN)